Appl. Phys. B 70, 91–97 (2000) / Digital Object Identifier (DOI) 10.1007/s003409900087

Applied Physics B
Lasers
and Optics

Calculation of the temperature distribution on laser-illuminated scanning probe tips

P.I. Geshev[1], **F. Demming**[2], **J. Jersch**[2], **K. Dickmann**[2]

[1] Institute of Thermophysics of Russian Academy of Sciences, Lavrentyev Ave.1, 630090 Novosibirsk, Russia
(Fax: +7-3832/357-880, E-mail: geshev@itp.nsc.ru)
[2] FH Muenster, FB Physikalische Technik, Laserlabor, Stegerwaldstr. 39, D-48565 Steinfurt, Germany
(Fax: +49-2551/149-201, E-mail: laserlab@fh-muenster.de)

Received: 14 October 1998/Accepted: 6 May 1999/Published online: 16 September 1999

Abstract. In order to understand the basic process of a laser-illuminated scanning probe tip it is necessary to calculate the temperature distribution in such a geometry. In the first part of this paper the temperature distribution in a laser-heated tip and a semi-infinite metallic sample is solved in a steady-state approach. This is done with the help of the boundary element method. In a second part, the temperature field in a thin metal sheet attached to a semi-infinite dielectric substrate is calculated by applying the Fourier–Bessel transformation method.

PACS: 02; 44.05.+e

A new and promising method for sample surface modification in the nanoscale region was proposed in [1, 2]. The pulsed laser illuminating of STM (scanning tunnel microscope) or SFM (scanning force microscope) probe tips, which are placed above a sample creates a series of nanocraters or nanogrooves on gold substrates. However, the main reason for the structuring process remains unclear and is controversially discussed by many groups [3–6]. To better understand the basic physical mechanism of this phenomenon it is necessary to estimate the temperatures of the sample and the tip. An appropriate method for the calculation of the electric fields on the tip, on the sample and in the free space has been developed as described in our previous paper [7]. This method is based on a quasi-steady-state (or electrostatic) approach. It means a reduction of the initial exact formulation of the problem (expressed through the Maxwell or Helmholtz equations) to the Laplace problem for the electric potential φ. This can be done due to the very small size of the region, in which the electric field is calculated. The region diameter should not exceed the Rayleigh size $R^* = \lambda/(2\pi)$, λ being the wavelength of the laser light. The phase shift in the field oscillations can be ignored for all points inside the domain of calculation. The electric field is expressed via the gradient of the complex electric potential φ, which is described in three domains I, II, III (sample , free space, and tip domain , respectively, see Fig. 1) by the Laplace equations

$$\Delta\varphi_s = 0, \quad \Delta\varphi_f = 0, \quad \Delta\varphi_t = 0. \tag{1}$$

On the outer boundaries of the spherical region (shown in Fig. 1) some appropriate boundary conditions were used following the exact Fresnel formulae.

The well-known continuity conditions for potentials and electric induction fields were used on the interface boundaries (S_1, S_3): .

$$\begin{aligned} &\text{on } S_1{:}\varphi_s = \varphi_f, \varepsilon_s\frac{\partial\varphi_s}{\partial n} = -\frac{\partial\varphi_f}{\partial n}, \\ &\text{on } S_3{:}\varphi_t = \varphi_f, \varepsilon_t\frac{\partial\varphi_t}{\partial n} = -\frac{\partial\varphi_f}{\partial n}, \end{aligned} \tag{2}$$

where ε_s, ε_t are the dielectric constants of sample and tip, respectively. The change of the direction of the normal vector for the inner and outer side of the surface causes the minus sign in (2). The problem (1), (2) can be transformed into a system of connected integral equations for the boundary values of the potentials φ and its normal derivatives $\frac{\partial\varphi}{\partial n}$. By applying the boundary element method [12–14] all integrals can be converted into discrete sums and solved directly by the Gauss method. A very large enhancement of the electric field

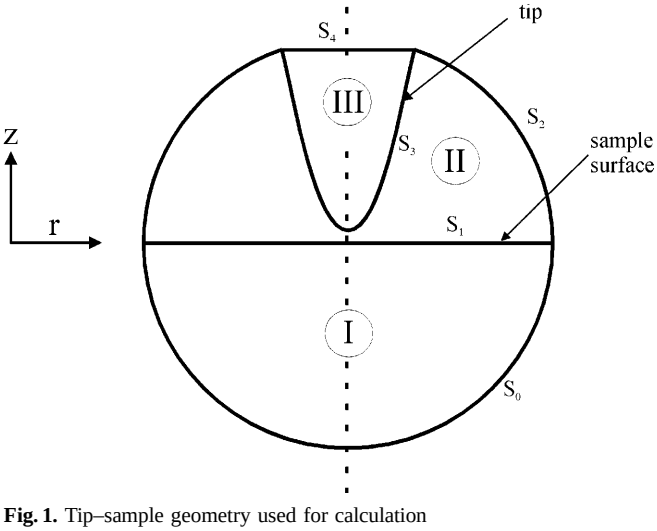

Fig. 1. Tip–sample geometry used for calculation

E was found near the apex of the probe. The field enhancement factor (FEF) determined as the ratio $E_{\max}/E_0$ (E_0 is the amplitude of the field in the incident laser beam) reaches values up to several hundred [7]. The FEF is a strong function of the tip-sample distance and the material properties of the tip and the sample (ε_s, ε_t).

In the first part of this paper the temperature distribution inside a laser-heated tip and a semi-infinite metallic sample is calculated by a steady-state approach. This is done with the help of the boundary element method.

In a second part, the temperature field inside a thin metal sheet attached to a semi-infinite dielectric substrate is calculated by applying the Fourier–Bessel transformation method.

1 Calculation of the temperature distributions in laser-illuminated sample and scanning probe tip of a tunneling microscope

1.1 Setting up the steady-state heat transfer problem

A penetrating electric field inside a tip or a sample causes a heat production according to the known formula [8]

$$Q = \frac{\omega_1}{8\pi}\varepsilon'' \mid \boldsymbol{E} \mid^2 \tag{3}$$

where Q is the volumetric density of the heat averaged over a period of the field, ε'' is the imaginary part of the complex dielectric constant of the tip or the sample material [9], ω_1 is the laser light frequency.

Why can we use the steady-state approach for the temperature calculation for a very short nanosecond heating pulse? The duration of the laser pulse is $\tau = (5\text{–}10) \times 10^{-9}$ sec, [1]. The thermo-diffusivity coefficient for typical metals is $a = (10^{-4}\text{–}10^{-5})\,\mathrm{m}^2/\mathrm{s}$ [10]. For $t \approx \tau$ the heat penetration length can be estimated as [11]

$$L = \sqrt{4a\tau} \approx 10^{-6}\,\mathrm{m}$$

This length is ten times larger than the distance used in our calculation (Rayleigh length $R^* \approx 100$ nm) and it is also two orders of magnitude larger than the tip curvature radius $R\mathrm{t} = (-)\,1030$nm. Therefore the steady-state approach can be applied.

With this approach the temperature in the tip and the sample is described by the Poisson equation:

$$\begin{aligned}\Delta T_t &= -\frac{Q_t}{\lambda_t} = -\frac{\omega_1 \varepsilon_t''}{8\pi\lambda_t} \mid E_t \mid^2,\\ \Delta T_s &= -\frac{Q_s}{\lambda_s} = -\frac{\omega_1 \varepsilon_s''}{8\pi\lambda_s} \mid E_s \mid^2,\end{aligned} \tag{4}$$

where λ_t, λ_s are the heat conductivity coefficients of tip and sample materials.

A transformation of (4) into a dimensionless form can be done by dividing all coordinates by the Raleigh scale R^*, and by using two temperature scales for tip and sample:

$$T_t^* = \frac{\lambda_1 \kappa_t n_t}{\pi\lambda_t} S_0, \quad T_s^* = \frac{\lambda_1 \kappa_s n_s}{\pi\lambda_s} S_0, \tag{5}$$

where κ_t, n_t, κ_s, n_s are the known optical constants (from handbook [9]) determined by the relations $\sqrt{\varepsilon_t} = n_t + \mathrm{i}\kappa_t$, $\sqrt{\varepsilon_s} = n_s + \mathrm{i}\kappa_s$, S_0 is the density of the energy flux in the laser beam (the modulus of the averaged Poynting vector). With a wavelength of $\lambda_l = 532$ nm, $S_0 = 10\,\mathrm{MW/cm^2}$ and a tungsten probe ($\lambda_t = 177\,\mathrm{W/(m^*K)}$)we come to $T_t^* = 908$ K. With a gold sample ($\lambda_t = 312\,\mathrm{W/(m^*K)}$) we come to $T_s^* = 61$ K. When we introduce dimensionless temperatures $\theta_t = T_t/T_t^*$, $\theta_s = T_s/T_s^*$ and coordinates we obtain

$$\Delta\theta_s = -\mid \nabla\varphi_s \mid^2, \quad \Delta\theta_t = -\mid \nabla\varphi_t \mid^2. \tag{6}$$

Here and hereunder φ_t and φ_s are the dimensionless electric potentials for the tip and the sample, described by Laplace equations (1) and (2). The right parts of equations (6) can be transformed by the formula

$$\mid \nabla\varphi \mid^2 = \Delta\frac{\mid \varphi \mid^2}{2}, \tag{7}$$

which is true for all harmonic functions.

Since the vector field $\nabla\varphi$ is also harmonic, it follows similar to (7):

$$\Delta \mid \nabla\varphi \mid^2 = 2 \mid \nabla\nabla\varphi \mid^2 > 0. \tag{8}$$

From (6)–(8) some important properties of φ, $\nabla\varphi$, and θ can be derived. Due to the positive left- and right-hand sides of (7) and (8) $\mid \varphi \mid^2$ and $\mid \nabla\varphi \mid^2$ can reach their maximum only on the boundaries, but not inside the regions. The temperature fields, according to the negative right-hand sides of (6), can have their minimum only on the boundary and not inside the region. These conclusions follow from the second condition for the maximum and minimum. All second derivatives should have the same sign, negative for maximum and positive for minimum.

The identity (7) permits us to transform the Poisson's problems (6) into Laplace problems

$$\Delta\Theta_s = 0, \quad \Delta\Theta_t = 0, \tag{9}$$

where the modified temperatures are:

$$\Theta_s = \theta_s + \frac{\mid \varphi_s \mid^2}{2}, \quad \Theta_t = \theta_t + \frac{\mid \varphi_t \mid^2}{2}. \tag{10}$$

This transformation (10) helps us to avoid Poisson's problem. We can use the boundary element method (BEM), to calculate the solutions for equations (9).

Let us consider the boundary conditions for the temperature fields θ_s and θ_t. Due to the zero heat conductivity within the free space between the sample and the tip, the adiabatic condition is applied on surfaces S_1 and S_3 (see Fig. 1):

$$\left.\frac{\partial\theta_s}{\partial n}\right|_{S_1} = 0, \quad \left.\frac{\partial\theta_t}{\partial n}\right|_{S_3} = 0. \tag{11}$$

On the boundaries S_0 and S_4 the heat flux density can be determined by the formula

$$\frac{\partial\theta}{\partial n} = -\frac{W}{\Omega R^2}. \tag{12}$$

W is the full amount of heat produced by the heat source Q in this region, Ω is the solid angle. For the probe cone $\Omega_t = 2\pi(1-\cos\theta_t)$ and for the semi-space $\Omega_s = 2\pi$, R is the radius of the control sphere as in Fig. 1. Formula (12) means that the heat W produced in a small domain near the tip apex (or near the origin of the system of coordinates for the semi-infinite sample) spreads for a relatively large distance (R) in a spherical symmetrical manner: the flux density is expected to be approximately constant on S_0 and S_4. In steady state, the heat produced by the heat source Q within the region flows through the boundary of the control sphere. In real experiments a much larger tip region is illuminated. This would mean an additional rise in temperature. However, the rise in temperature which is due to laser illumination is much higher for the tip apex than for the upper tip region. Therefore, from (12) a formula for the temperature on S_0 and S_4 can be found by integrating over R.

$$\theta = \frac{W}{\Omega R}. \tag{13}$$

For the heat W produced in the volume of the tip or the sample we can derive the following formula:

$$W = \int\limits_V |\nabla\varphi|^2 \mathrm{d}V = \oint\limits_S \frac{\partial}{\partial n}\frac{|\varphi|^2}{2}\mathrm{d}S = \oint\limits_S \mathrm{Re}\left\{\varphi^*\frac{\partial\varphi}{\partial n}\right\}\mathrm{d}S. \tag{14}$$

The final expression (14) for the heat W contains only the boundary values of φ^* and $\frac{\partial\varphi}{\partial n}$, which are calculated with the help of BEM [7].

Finally the boundary conditions for the modified temperatures Θ_s and Θ_t are

$$\text{on } S_1 : \frac{\partial\Theta_s}{\partial n} = \mathrm{Re}\left\{\varphi_s^*\frac{\partial\varphi_s}{\varphi n}\right\}, \text{on } S_0 : \Theta_s = \frac{W_s}{2\pi R} + \frac{|\varphi_s|^2}{2}, \tag{15}$$

$$\begin{aligned}&\text{on } S_3 : \frac{\partial\Theta_t}{\partial n} = \mathrm{Re}\left\{\varphi_t^*\frac{\partial\varphi_t}{\varphi n}\right\},\\ &\text{on } S_4 : \Theta_t = \frac{W_t}{2\pi(1-\cos\theta_t)R} + \frac{|\varphi_t|^2}{2}.\end{aligned} \tag{16}$$

1.2 Boundary element method for solution of the Laplace problem

The Laplace equations (9) can effectively be solved by the BEM [7, 12–14]. The mathematical details of the BEM for axis-symmetrical problems can be found in [7]. The following expression can be derived:

$$\begin{aligned}\alpha\Theta(\boldsymbol{R}) + \int\limits_\Gamma \frac{\partial F(\boldsymbol{R},\boldsymbol{R}')}{\partial n}\Theta(\boldsymbol{R}')r'\mathrm{d}\Gamma(\boldsymbol{R}')\\ = \int\limits_\Gamma F(\boldsymbol{R},\boldsymbol{R}')\frac{\partial\Theta(\boldsymbol{R}')}{\theta n}r'\mathrm{d}\Gamma(\boldsymbol{R}'),\end{aligned} \tag{17}$$

and

$$\begin{aligned}&F(\boldsymbol{R},\boldsymbol{R}') = \frac{K(c)}{\pi(a+b)^{1/2}}, \quad \boldsymbol{R} = (r,z), \quad \boldsymbol{R}' = (r',z'),\\ &\frac{\partial F(\boldsymbol{R},\boldsymbol{R}')}{\partial n} = \frac{E(c)-K(c)}{2\pi r'(a+b)^{1/2}}n_r\\ &\qquad + \frac{n_r(r-r') + n_z(z-z')}{\pi(a-b)(a+b)^{1/2}}E(c),\\ &a = r^2 + r'^2 + (z-z')^2,\ b = 2rr',\ c^2 = \frac{4rr'}{(r+r')^2+(z-z')^2}.\end{aligned} \tag{18}$$

F is the Greens Function for axis-symmetrical problems. E and K are elliptic integrals of the first and second kind [12–14] and Γ is the boundary line of the domain.

Equations (17) and (18) together with the boundary conditions (15) and (16) can be used as a starting point for the numerical calculation of the temperature distribution with BEM. This is done by taking points $\boldsymbol{R}$ on the boundary S and by replacing equation (17) with its discrete form

$$\begin{aligned}\alpha_i\Theta_i + \sum_{j=1}^{N}\Theta_j\int\limits_{s_j}\frac{\partial F(\boldsymbol{R}_i,\boldsymbol{R}_j)}{\partial n_j}\mathrm{d}s_j =\\ \sum_{j=1}^{N}\left(\frac{\partial\Theta}{\partial n}\right)_j\int\limits_{s_j}F(\boldsymbol{R}_i,\boldsymbol{R}_j)\,\mathrm{d}s_j.\end{aligned} \tag{19}$$

For all boundary points $\boldsymbol{R}$ the integrals under the sum can be calculated numerically over a small boundary element s_j because the solution for $F(\boldsymbol{R},\boldsymbol{R}')$ is known. The integrals in (19) will be:

$$G_{ij} = \int\limits_{\Gamma_j} Fr'\mathrm{d}\Gamma, \quad H_{ij} = \int\limits_{\Gamma_j}\frac{\partial F}{\partial n}r'\mathrm{d}\Gamma. \tag{20}$$

These integrals were calculated numerically in the meridian plane Γ by Gauss method [14]. They are the elements of the global matrix equation for two non-connected Laplace problems for domains I and III:

$$H_{ij}\Theta_j = G_{ij}q_j, \tag{21}$$

where q_j designates the normal derivative of Θ on the j-th boundary element. The diagonal element with α_i is included in H_{ij}.

Figure 2 shows the temperature distribution along the tip and sample boundary for different geometry and tip materials (tungsten and silver tip, gold surface $\lambda = 532$ nm, $S_0 = 10\,\mathrm{MW/cm^2}$). The temperature in both domains depends to a great extent on the tip's geometry and material. For tungsten tips, the temperature in the tip is 1–2 orders of magnitude larger than in the sample. The main reason for this difference is the large volume of the sample in which the heat is distributed and also the much better heat conductivity of the gold sample. Moreover the absorption coefficient (the imaginary part of the dielectric constant) is much larger for tungsten.

As expected, for a larger tip volume, the temperature decreases in the tip whereas the temperature in the sample volume increases. For the chosen larger tip geometry, the

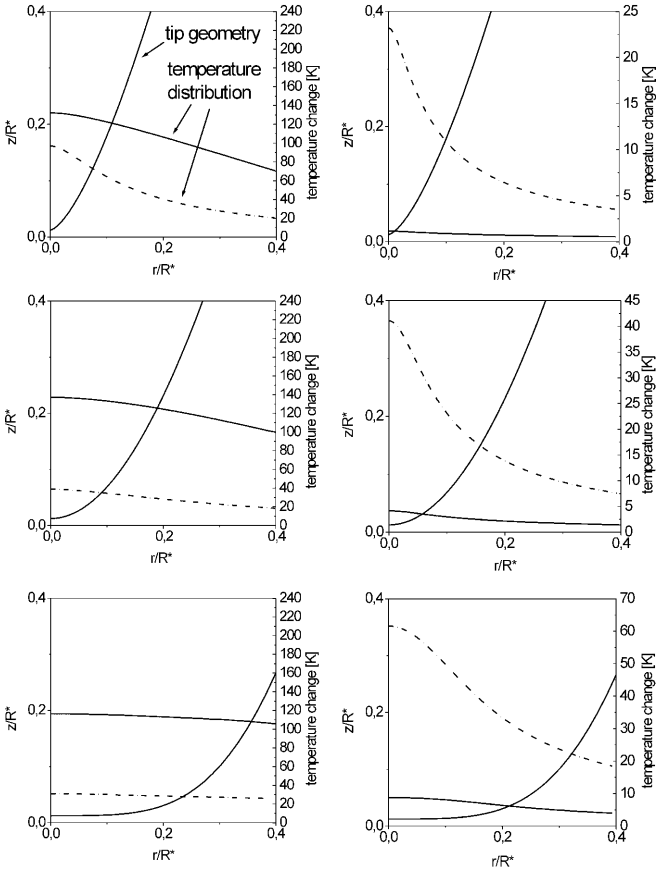

Fig. 2. Temperature distribution along the tip (*left side*) and sample boundary (*right side*) for different geometries. (tungsten tip *solid line*, silver tip *dotted line*, gold surface $\lambda = 532\,\mathrm{nm}$, $S_0 = 10\,\mathrm{MW/cm^2}$)

FEF decreases [7]. Simultaneously, the enhanced field is distributed over a larger volume. A larger overall heat production in the sample volume is the consequence.

The situation is different for silver tips. For a certain tip geometry the temperature in the sample can exceed the temperature in the tip. There are several reasons. The field enhancement of silver tips is usually much larger than the FEF of tungsten. Additionally, silver has a much smaller absorption (at this wavelength) and a much better heat conductivity than tungsten. Therefore, the equilibrium between produced heat and heat flow out of the tip region is reached at a smaller temperature.

2 Calculation of the temperature distribution in thin metal sheets

As mentioned above it was shown that the heat produced in a metallic semi-infinite sample spreads quickly over a large volume and the temperature of the sample is not very high. If the sample is made of a thin metal sheet with a high heat conductivity λ_s placed on a dielectric with a small heat conductivity $\lambda_\mathrm{d}(\lambda_\mathrm{d} < \lambda_\mathrm{s})$ changes. When the heat conductivity of the support is zero ($\lambda_\mathrm{d} = 0$), the steady-state solution of the heat transfer problem cannot exist. This means that the temperature of the sheet in the two-dimensional case rises to infinity during an infinite period of time. In the case of a small λ_d one can expect that the heat encounters a much larger thermal resistance while spreading over the thin sheet which leads to a higher temperature.

Let us consider this non-steady-state problem. The time dependencies of the light intensity S_0 and of the heat source Q can be described as a Gauss curve

$$Q(t, \boldsymbol{r}) = q(\boldsymbol{r})\mathrm{e}^{-t^2/\tau^2}$$

where τ is the characteristic laser pulse duration. The equations for the temperature fields in the sheet and in the dielectric support are

$$\Delta T_\mathrm{s} - \frac{1}{a_\mathrm{s}}\frac{\partial T_\mathrm{s}}{\partial t} = -\frac{q(\boldsymbol{r})}{\lambda_\mathrm{s}}\mathrm{e}^{-t^2/\tau^2},\ \Delta T_\mathrm{d} - \frac{1}{a_\mathrm{d}}\frac{\partial T_\mathrm{d}}{\partial t} = 0. \tag{22}$$

(a_s, a_d are the thermo-diffusivity coefficient of the metal surface and the dielectric support, respectively). After applying the integral Fourier transformation (designated below by '$\sim$') to system (22) we get

$$\Delta\tilde{T}_\mathrm{s} - \frac{\mathrm{i}\omega}{a_\mathrm{s}}\tilde{T}_\mathrm{s} = -\frac{q(\boldsymbol{r})\tau}{\lambda_\mathrm{s}2\sqrt{\pi}}\mathrm{e}^{-(\omega\tau/2)^2},\quad \Delta\tilde{T}_\mathrm{d} - \frac{\mathrm{i}\omega}{a_\mathrm{d}}\tilde{T}_\mathrm{d} = 0. \tag{23}$$

The boundary conditions are

$$\text{at}\quad z = 0\text{:}\quad \frac{\partial\tilde{T}_\mathrm{s}}{\partial z} = 0, \tag{24}$$

$$\text{at}\quad z = -H\text{:}\quad \tilde{T}_\mathrm{s} = \tilde{T}_\mathrm{d},\quad \lambda_\mathrm{s}\frac{\partial\tilde{T}_\mathrm{s}}{\partial z} = \lambda_\mathrm{d}\frac{\partial\tilde{T}_\mathrm{d}}{\partial z}, \tag{25}$$

at infinity, $\sqrt{\rho^2 + z^2} \to \infty : \tilde{T}_\mathrm{s} = \tilde{T}_\mathrm{d} = 0$.

Assuming a sufficiently quick decay of all used functions at $\rho \to \infty$ the Hankel integral transformation can be applied to the problem:

$$\tilde{T}(\rho, z) = \int_0^\infty \hat{T}(k, z)\, J_\nu(k\rho) k\,\mathrm{d}k,$$

$$\hat{T}(k, z) = \int_0^\infty \tilde{T}(\rho, z)\, J_\nu(k\rho) k\,\mathrm{d}\rho. \tag{26}$$

For our problem: $\nu = 0$.

Dimensionless coordinates, time, frequency, and source function are introduced via the scales R^* and τ. We use: $\rho' = \rho/R^*$, $k' = kR^*$, $z' = z/R^*$, $t' = t/\tau$, $\omega' = \omega\tau$, $H' = H/R^*$. The source function f is determined by

$$\tilde{f}(\rho, z) = \frac{{R^*}^2}{T_\mathrm{s}^*}\frac{q(\boldsymbol{r})}{\lambda_\mathrm{s}2\sqrt{\pi}}\mathrm{e}^{-(\omega\tau/2)^2}.$$

Below, the prime $'$ will be omitted.

The governing system of equations for the dimensionless temperatures is:

$$\frac{\mathrm{d}^2\hat{\theta}_\mathrm{s}}{\mathrm{d}z^2} - \kappa_\mathrm{s}^2\hat{\theta}_\mathrm{s} = -\hat{f}\quad (0 > z > -H),$$

$$\frac{\mathrm{d}^2\hat{\theta}_\mathrm{d}}{\mathrm{d}z^2} - \kappa_\mathrm{d}^2\hat{\theta}_\mathrm{d} = 0\quad (z < -H), \tag{27}$$

where κ_s, κ_d are also dimensionless:

$$\kappa_s = \sqrt{k^2 + i\omega/Fo_s}, \quad \kappa_d = \sqrt{k^2 + i\omega/Fo_d}. \tag{28}$$

The combinations $\frac{a_s\tau}{R^{*2}} = Fo_s$ and $\frac{a_d\tau}{R^{*2}} = Fo_d$ are called the Fourier criteria in heat transfer theory. Equation (27) can be solved in a general form

$$\hat{\theta}_s = I\frac{e^{-\kappa_s H}(1-\Lambda)}{\kappa_s \Phi} ch(\kappa_s z) + \frac{1}{2\kappa_s}\int_0^H \left[e^{-\kappa_s|z'-z|} + e^{-\kappa_s(z'+z)}\right]\hat{f}(k,z')dz',$$

$$\hat{\theta}_d = I\frac{e^{-\kappa_d(z-H)}}{\kappa_s\Phi}, \tag{29}$$

where

$$\Phi = \Lambda ch(\kappa_s H) + sh(\kappa_s H), \quad \Lambda = \frac{\lambda_d\kappa_d}{\lambda_s\kappa_s},$$

$$I = \int_0^H ch(\kappa_s z')\,\hat{f}(k,z')dz', \tag{30}$$

$$\hat{f}(k,z') = \int_0^\infty \tilde{f}(\rho',z')\,J_0(k\rho')\rho' d\rho'. \tag{31}$$

The integrals (30) and (31) can be substituted into expressions (29). After applying the back Hankel transformation the temperatures in the sheet and in the dielectric support can be obtained

$$\tilde{\theta}_s(z=0,\rho) = \int_0^\infty \rho' d\rho' \int_0^\infty dk \frac{J_0(k\rho)J_0(k\rho')}{\kappa_s} \times \int_0^H \left[e^{-\kappa_s z'} + \frac{(1-\Lambda)}{\Phi}e^{-\kappa_s H}ch(\kappa_s z')\right]\tilde{f}(\rho',z')dz',$$

$$\tilde{\theta}_d(z=-H,\rho) = \int_0^\infty \rho' d\rho' \int_0^\infty dk \frac{J_0(k\rho)J_0(k\rho')}{\kappa_s\Phi} \times \int_0^H ch(\kappa_s z')\,\tilde{f}(\rho',z')dz'. \tag{32}$$

These temperatures are in the frequency domain. The inverse Fourier transformation can be applied to obtain these values in the time domain. Fast Fourier Transformation (FFT) can be used for this purpose.

In order to understand the obtained results we now use a simplified form for the inner integral. For electromagnetic waves propagating in a conducting metal, the intensity decreases exponentially according to Fresnel's formula. The decay coefficient is given by:

$$\gamma = 2\sqrt{\sin^2\theta_{beam} - \varepsilon},$$

where θ_{beam} is the angle between the light beam and the direction normal to the surface. The same behavior can be supposed for the heat production in the sheet

$$\tilde{f}(\rho,z) = \tilde{f}_0(\rho)e^{-\gamma z}. \tag{33}$$

The inner integral in expression (32) can be calculated obtaining.

$$\tilde{\theta}_s(z=0,\rho) = \int_0^\infty \tilde{f}_0(\rho')\rho' d\rho' \int_0^\infty \frac{J_0(k\rho)J_0(k\rho')}{\kappa_s(\kappa_s+\gamma)} \left\{1 + \frac{(1-\Lambda)\gamma}{\Phi}\left[\frac{e^{-\gamma H} - e^{-\kappa_s H}}{\kappa_s - \gamma}\right] - \frac{\Lambda}{\Phi}e^{-\gamma H}\right\} k dk$$

$$\tilde{\theta}_d(z=-H,\rho) = \int_0^\infty \tilde{f}_0(\rho')\rho'\,d\rho' \int_0^\infty \frac{J_0(k\rho)J_0(k\rho')}{\kappa_s(\kappa_s+\gamma)\Phi} \left\{\gamma ch(\kappa_s H)\left[\frac{e^{-\gamma H} - e^{-\kappa_s H}}{\kappa_s - \gamma}\right] - sh(\kappa_s H)\left[\frac{\kappa_s e^{-\gamma H} - \gamma e^{-\kappa_s H}}{\kappa_s - \gamma}\right]\right\} k\,dk\,. \tag{34}$$

For the steady-state solution $\omega = 0$ and $\kappa_s = \kappa_d = k$. For small $k(k \ll 1)$ and small $\Lambda(\Lambda \ll 1)$ the value $\Phi = \Lambda + kH$ is very small and the integrals in (34) become divergent at $\Lambda = 0$. Only at nonzero heat conductivity of the support may a finite temperature field be obtained. This conclusion illustrates the above-discussed important general features of our solutions (the steady-state solution does not exist in the two-dimensional case).

The integrals in (32) were calculated numerically. The Hankel integral was solved by the Newton–Cotes adoptive algorithm [15]. The integrals in ρ and z were found by the trapeze method. The inverse Fourier transformation in the non-steady-state case was done by the help of FFT.

First off all we want to consider the results for the steady-state case. Figure 3 shows the radial temperature distribution along the layer surface (solid line) and the layer-support boundary (dotted line) (layer thickness $H = 0.1$ and $0.17\ R^*$) The corresponding tip geometry can be found in Fig. 2a. For thin layer ($H = 0.1$) only a minor difference between the radial temperature distribution at upper ($z = 0$) and lower ($z = -H$) boundary of the metal film can be found.

Now the result for the non-steady-state model is calculated and shown in Fig. 4 in comparison with the solution obtained in the quasi-steady-state approach (the quasi-steady-state approach gives the maximum temperature in the sheet for large pulse length). The picture shows the results for different sheet thickness H. For thin films only a minor difference between the steady state and the non-steady-state solution can be found. In addition, the temperature distribution for the upper and lower boundary of the metal film are almost identical in steady and non-steady-state case and lines for the upper and lower boundary temperature distribution merge into one. Having a larger film thickness we can see some damping of the temperatures and the appearance of temporal tails compared to the quasi-steady-state results. A temperature difference between upper and lower boundary can be noted.

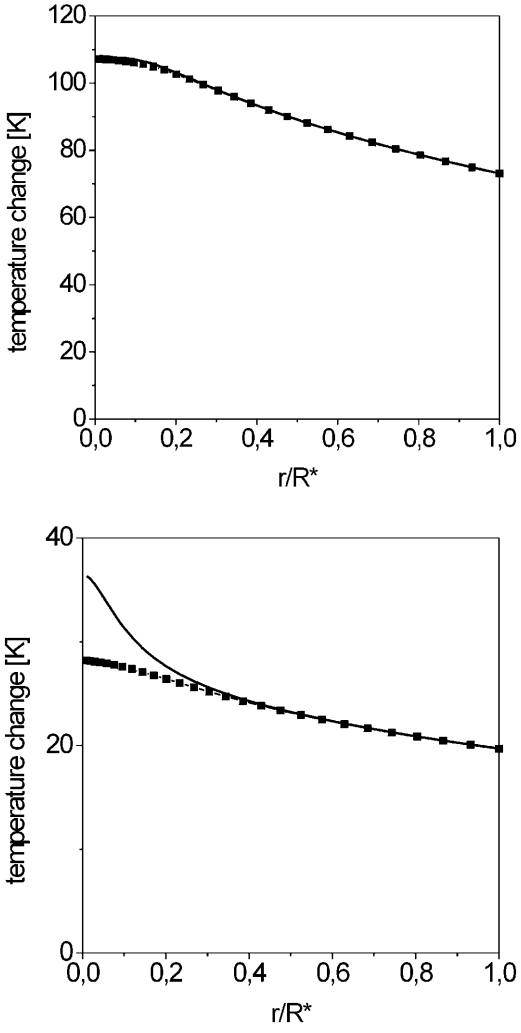

Fig. 3. Temperature in the metallic sheet: at $z = 0$ (*solid line*), $z = -H$ (*dotted line*), (tungsten tip, gold sample, $H = 0.1$ and $0.17R^*$, respectively, $S_0 = 10\,\mathrm{W/cm^2}$, $\lambda_d/\lambda_s = 0.01$). For thin layer ($H = 0.1$) only a minor difference between the radial temperature distribution at upper and lower boundary of the metal film can be found

3 Conclusions

The steady-state solution of the heat transfer problem for a tip and a metallic semi-infinite space was transformed into a Laplace problem and solved by the boundary element method (BEM). BEM was also applied in the calculations of the electric fields in our previous and in the current papers. A very large field enhancement factor (FEF) was found in our previous calculations. This large FEF causes a large heat production in a very small region of nanometer size near the tip apex.

We noted that the rise of temperature of a tungsten probe tip is one to two orders of magnitude higher than the maximum temperature of the sample. This is in agreement with the conclusion drawn in [16], where a different approach for the investigated problem was developed. For silver tips, the situation is different. For a certain geometry, the temperature in the sample can be in the same order of magnitude as the temperature on the tip due to the smaller absorption and the better heat conductivity.

Similar to results of [16] the tungsten tip temperature in our calculations can rise by about one hundred degree, while a massive sample can reach only several degree. The main reason for this difference is the large volume of the sample where the heat is distributed. In other words there is a large solid angle of the sample relative to the one of the probe cone. When this volume decreases, a increasing temperature within the sample can be expected.

Such a decrease happens when a thin metal sheet attached to a dielectric support with small heat conductivity is considered. This problem was solved analytically for the non-steady-state case. We used the integral Fourier transformation in time and Hankel transformation in radial coordinates. An analysis of the analytical solution shows that the temperature of the metal sheet has a logarithmic divergence in the inverse Hankel transformation if the heat conductivity of the dielectric support is zero. This is in accordance with the known conclusion of the heat transfer theory. The two-dimensional Laplace problem has no solution in the case of an infinite space.

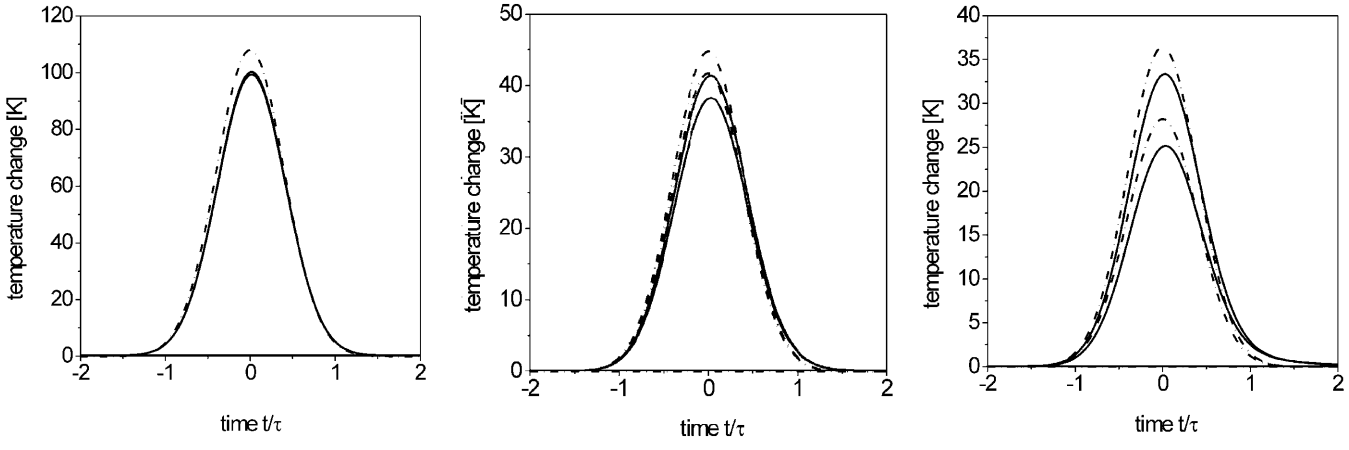

Fig. 4. Comparison of the results for steady-state (*dotted line*) and non-steady-state (*solid line*) models (for $z = 0$, and $z = -H$; at $\rho = 0$, tungsten tip, gold sample, $\lambda_d/\lambda_s = 0.01$, $H = 0.1, 0.17, 0.27$, respectively). For $H = 0.1$ for thin films only a minor difference between the steady-state and the non-steady-state solution can be found. In addition, the temperature distribution for the upper and lower boundary of the metal film are almost identical in steady and non-steady-state case. The *lines* for the upper and lower boundary temperature distribution merge into one. For larger film thickness ($H = 0.17, 0.27$) a damping of the temperatures and the appearance of temporal tails in the non-steady-state in comparison to the quasi-steady-state can be found. Also a temperature difference between upper and lower boundary can be seen

The maximum temperature of the confined metallic sheet is much higher than for the semi–infinite space. The temperature can reach several hundred degrees. The effect depends strongly on the material properties of the tip and the sample. The geometry parameters of the problem (the tip–sample distance, the curvature radius of the tip, the angle of the laser beam, and the solid angle of the probe cone) also have great influence on the final results.

The non-steady-state model for heat transfer in the metal sheet shows a considerable decrease of the maximal temperature in comparison with the temperatures found in the steady-state approach. Small shifts of the temperature profiles in time and temporal tails are also found in the non-steady-state results.

Finally, we can suppose that applying this problem to quasi-one- or quasi-zero-dimensional nano-structures placed on a dielectric support with small heat conductivity will cause much higher temperatures of the samples than we even calculated in this paper. It means that nano wires and small thin confined objects having nanometer size can reach melting or evaporation temperature while the tip is still far away from this temperature. Such materials can be successfully cut, welded, and soldered. This makes the method flexible and an important tool for nano structuring.

Acknowledgements. This work is supported by the Deutsche Forschungsgemeinschaft (DFG) under Grant No.: Di 456.

References

1. A.A. Gorbunov, W. Pompe: Phys. Status Solidi A **145**, 333 (1994)
2. J. Jersch, K. Dickmann: Appl. Phys. Lett. **68**(6), 868 (1996)
3. I. Lyubinetsky, Z. Dohnálek, V.A. Ukraintsev, J.T. Yates, Jr.: J. Appl. Phys. **82**, 4115 (1997)
4. S. Grafström, P. Schuller, J. Kowalski, R. Neumann: J. Appl. Phys. **83**, 3453 (1998)
5. J. Boneberg, M. Tresp, M. Ochmann, H.J. Münzer, P. Leiderer: Appl. Phys. A **66**, 615 (1998)
6. R. Huber, M. Koch, J. Feldmann: Appl. Phys. Lett. **73**, 2521 (1998)
7. F. Demming, J. Jersch, K. Dickmann, P.I. Geshev: Appl. Phys. B **66**, 593 (1998)
8. L.D. Landau, E.M. Lifschitz: *Elektrodynamik der Kontinua*, 3rd edition (Akademie, Berlin 1980)
9. E.D. Palik (Ed.): *Handbook of Optical Constants of Solids* (Academic Press, New York 1985)
10. R.C. Weast (Ed.): *CRC Handbook of Chemistry and Physics*, 69th edn. (CRC, Roca Button 1989)
11. V. A Ukraintsev, J.T. Yates, Jr.: J. Appl. Phys. **80**(5), 2561 (1996)
12. C.A. Brebbia, J.C.F. Telles, L.C. Wrobel: *Boundary Element Techniques. Theory and Applications in Engineering* (Springer, Berlin, New York 1984)
13. P.K. Banerjee, R. Batterfield: *Boundary Element Method in Engineering Science* (McGraw-Hill, London 1981)
14. P.K. Kythe: *Boundary Element Methods* (CRC Press, London 1995)
15. G.E. Forsyte, M.A. Malcolm, C.B. Mouler: *Computer Methods for Mathematical Computations* (Prentice-Hall, NJ 1977)
16. N.M. Miskovsky, S.H. Park, J. He, P.H. Cutler: J. Vac. Sci. Technol. B **11**(2), 366 (1993)